Nonlinear band structure in Bose-Einstein condensates: Nonlinear Schrödinger equation with a Kronig-Penney potential

B. T. Seaman, L. D. Carr, and M. J. Holland
JILA, National Institute of Standards and Technology and Department of Physics, University of Colorado, Boulder, Colorado 80309-0440, USA
(Received 13 October 2004; published 21 March 2005)

All Bloch states of the mean field of a Bose-Einstein condensate in the presence of a one-dimensional lattice are presented in closed analytic form. The band structure is investigated by analyzing the stationary states of the nonlinear Schrödinger, or Gross-Pitaevskii, equation for both repulsive and attractive condensates. The appearance of swallowtails in the bands is examined and interpreted in terms of the condensates superfluid properties. The nonlinear stability properties of the Bloch states are described and the stable regions of the bands and swallowtails are mapped out. We find that the Kronig-Penney potential has the same properties as a sinusoidal potential. Bose-Einstein condensates are trapped in sinusoidal optical lattices. The Kronig-Penney potential has the advantage of being analytically tractable, unlike the sinusoidal potential, and, therefore, serves as a good model for understanding experimental phenomena.

DOI: 10.1103/PhysRevA.71.033622 PACS number(s): 03.75.Hh, 03.75.Lm, 03.65.Ge

I. INTRODUCTION

Periodic potentials are ubiquitous in physics, appearing in electron transport in metals [1], Josephson junction arrays [2], nonlinear photonic crystals and waveguide arrays [3], and Bose-Einstein condensates (BEC's) [4]. With the realization of BEC's of alkali-metal atoms in a sinusoidal optical lattice, there has been an explosion in studies of BEC's in periodic potentials, both experimentally and theoretically [5–10]. BEC's in periodic potentials have been used to study phase coherence of atom lasers [11,12] and matter-wave diffraction [13]. Therefore, in the context of the BEC, the study of periodic potentials provides an excellent connection between condensed matter physics and atomic physics. In contrast to other physical contexts, the lattice geometry and strength, as well as the interatomic interactions [14,15], are all tunable parameters for the BEC. We show that the mean-field Bloch states of a BEC in a Kronig-Penney potential, i.e., a lattice of δ functions, exhibit the same band structure and stability properties as the experimental case of a sinusoidal potential. Unlike in the case of the sinusoidal potential, Bloch state solutions to the Kronig-Penney potential can be described by straightforward analytic expressions. The Kronig-Penney potential, therefore, has distinct advantages as a model of BEC's trapped in periodic potentials.

Specifically, we consider the steady-state response of the mean field of a BEC to a Kronig-Penney potential using the Bloch ansatz. The mean field is modeled by the nonlinear Schrödinger equation (NLS), which appears in numerous areas of physics; in the context of the BEC, it is often called the Gross-Pitaevskii equation [16,17]. We have previously obtained the full set of stationary solutions for a single δ function analytically [18–21]. Using these results, we are able to rigorously describe the band structure. We find that above a critical nonlinearity, swallowtails, or loops, form in the bands [22,23]. These swallowtails are related to superfluid properties of the BEC [24], as we shall explain. Stability properties are studied numerically by time evolution of perturbed stationary-state solutions to the NLS. It is found that stable, as well as unstable, regimes exist for both repulsive and attractive BEC's.

Experimentally, in order to create a BEC in a lattice, alkali-metal atoms are first cooled to a quantum degenerate regime by laser cooling and evaporation in harmonic electromagnetic traps [25,26]. A sinusoidal optical lattice is then made by the interference of two counter-propagating laser beams, which creates an effective sinusoidal potential proportional to the intensity of the beams [5]. The potential is due to the ac Stark shift induced by the dipole interaction with the electromagnetic field on the atoms' center of mass [27]. For large detuning of the optical field from the atomic transition, dissipative processes, such as spontaneous emission, can be minimized and the potential becomes conservative. Nonzero quasimomentum can be examined by slightly detuning the two lasers relative to each other by a frequency $\delta\nu$ [10]. The resulting interference pattern is then a traveling wave moving at the velocity $v=(\lambda/2)\delta\nu$, where λ is the wavelength of the first beam. This produces a system with quasimomentum $q=mv/\hbar$, where m is the atomic mass. After a given evolution time, the traps are switched off. The BEC is allowed to expand and the density is then imaged.

The case of a BEC trapped in a sinusoidal potential has been studied theoretically in great detail by a number of researchers [22–24,28–44]. In addition, a subset of the solutions to the Kronig-Penney potential has been found [45–49]. Recently, for example, Li and Smerzi [49] investigated generalized Bloch states for constant phase and zero current. In contrast, we present the full set of Bloch-wave stationary solutions for both repulsive and attractive BEC's. An important point is that the sinusoidal optical lattice potential is composed of a single Fourier component. If more counter-propagating laser beams of different frequencies are added as is experimentally possible, more Fourier components are introduced, and the potential becomes a lattice of well separated peaks. In the limit that the width of the these peaks becomes much smaller than the healing length of the BEC,

the potential effectively becomes a Kronig-Penney lattice. However, we show that the Kronig-Penney potential serves as a good model even for experiments with a single Fourier component.

The article is organized as follows. In Sec. II, the Bloch-wave solutions to the stationary NLS with a Kronig-Penney potential are presented. The energy bands are detailed for repulsive and attractive condensates in both the weakly and strongly interacting regimes in Sec. III. In Sec. IV, the changes in the density profile of the condensate are examined as the quasimomentum changes. The stable and unstable regimes of the bands are studied in detail for both repulsive and attractive condensates in Sec. V. Finally, concluding remarks are made in Sec. VI.

II. NONLINEAR SCHRÖDINGER EQUATION AND BLOCH WAVES

We consider the mean-field model of a quasi-one-dimensional (quasi-1D) BEC in the presence of a Kronig-Penney potential,

$$V(x) = V_0 \sum_{j=-\infty}^{+\infty} \delta(x-j), \tag{1}$$

where length has been rescaled by the lattice spacing d and V_0 is the strength of the potential. When the transverse dimensions of the BEC are on the order of its healing length and its longitudinal dimension is much longer than its transverse ones, the 1D NLS [50,51] which describes the stationary states of the mean field of a BEC is given by

$$-\frac{1}{2}\Psi_{xx} + g|\Psi|^2\Psi + V(x)\Psi = \mu\Psi. \tag{2}$$

Here μ is the eigenvalue, g characterizes the short-range pairwise interaction, and $V(x)$ is an external potential [52]. In the case where the harmonic oscillator length approaches the s-wave scattering length $a_s \propto g$, the 1D NLS no longer models the system and a one-dimensional field theory with the appropriate effective coupling constant must be considered instead [52]. Since a_s is on the scale of hundreds of angstroms for typical BEC's, this regime is not relevant to the present study.

In Eqs. (1) and (2), the length is scaled according to the lattice spacing d, and the energy has been rescaled by $\pi^2/(2E_0)$, where

$$E_0 \equiv \frac{\hbar^2\pi^2}{2md^2} \tag{3}$$

is the kinetic energy of a particle with a wave vector equal to that at the boundary of the first Brillouin zone, where m is the atomic mass. The variables in Eq. (2) are defined by

$$x = \frac{1}{d}x', \tag{4}$$

$$\mu = \frac{\pi^2}{2E_0}\mu', \tag{5}$$

$$g = \frac{\pi^2}{2E_0}g', \tag{6}$$

$$V(x) = \frac{\pi^2}{2E_0}V'(x'/d), \tag{7}$$

where the primed variables contain the physical units of the system. The renormalized 1D coupling is $g \equiv a_s\omega md/\hbar$, where a harmonic oscillator confinement in the transverse directions has been assumed with frequency ω. Both attractive and repulsive atomic interactions, i.e., $g>0$ and $g<0$ shall be considered. The wave function or order parameter $\Psi(x,t)$ has the physical meaning

$$\Psi(x,t) = \sqrt{\rho(x,t)}\,\exp[-i\mu t + i\phi(x,t)], \tag{8}$$

where $\rho(x,t)$ is the line density and the local superfluid velocity is given by $v(x,t) = \partial\phi(x,t)/\partial x$.

In addition to the NLS, Eq. (2), the normalization of the wave function is given by

$$n = \int_0^1 \rho(x)\mathrm{d}x, \tag{9}$$

where n is the number of atoms per lattice site. The boundary conditions induced by the Kronig-Penney potential cause a discontinuity in the derivative of the wave function across each δ function,

$$\lim_{\epsilon\to 0}[\partial_x\rho(j+\epsilon) - \partial_x\rho(j-\epsilon)] = 4V_0\rho(0), \tag{10}$$

where j is an integer.

A brief review is now given of the general solution to Eq. (2) with no external potential. We have previously presented a proof that this represents the full set of solutions for a constant potential [18]. Therefore, by using this complete set of stationary state solutions to the constant potential case, we can calculate the full set of Bloch solutions for a lattice.

The density ρ and the phase ϕ, which solve Eq. (2) for a constant potential, are

$$\rho(x) = B + \frac{k^2b^2}{g}\mathrm{sn}^2(bx + x_0, k), \tag{11}$$

$$\phi(x) = \alpha\int_0^x \frac{1}{\rho(x)}\mathrm{d}x, \tag{12}$$

where sn is a Jacobi elliptic function [53,54]. The density offset B, the horizontal scaling b, the translational offset x_0, and the elliptic parameter k are free variables. The Jacobi elliptic functions are generalized periodic functions characterized by an additional parameter $k \in [0,1]$. In the limit that $k\to 0$ and $k\to 1$ the Jacobi elliptic functions become circular and hyperbolic trigonometric functions, respectively. The period of the square of the Jacobi elliptic functions is given by $K(k)\epsilon[\pi,\infty)$, where $2K(k)$ is a complete elliptic integral of the first kind [53,54].

Substituting Eqs. (11) and (12) into Eqs. (8) and (2), with $V(x)=0$, one finds that the eigenvalue μ and phase prefactor α are given by

$$\mu = \frac{1}{2}(b^2(1+k^2) + 3Bg), \tag{13}$$

$$\alpha^2 = B(k^2b^2/g + B)(b^2 + Bg). \tag{14}$$

The boundary conditions are used to determine the appropriate values of the free variables B, b, x_0, and k.

In this article, we use the methods from our previous paper [18] and apply them to a situation in which a lattice of δ functions is present. We seek Bloch-wave solutions of the form

$$\Psi(x) = e^{iqx} f_q(x), \tag{15}$$

where q is the wave number, $\hbar q$ is the quasimomentum, and $f_q(x)$ has the same period as the lattice, $f_q(x) = f_q(x+1)$. By substituting Eq. (15) into Eq. (8), one finds that the density ρ must also have the same period as the lattice and that the wave number and energy per particle can be determined from the density profile by

$$q = \int_0^1 \frac{\alpha}{\rho(x)} \mathrm{d}x, \tag{16}$$

$$\frac{E[\Psi]}{n} = \frac{1}{n}\int_0^1 \mathrm{d}x \left(\frac{1}{2}|\Psi_x|^2 + \frac{g}{2}|\Psi|^4 + V_0\delta(x)|\Psi|^2 \right). \tag{17}$$

The quasimomentum is simply the phase jump across each lattice site and corresponds to the momentum proportional to the average superfluid velocity of the system,

$$q = \langle v(x) \rangle = \langle \partial\phi(x)/\partial x \rangle. \tag{18}$$

We examine the quasimomentum-energy bands. The problem, therefore, reduces to one in which the density is symmetric around the middle of the lattice sites, $x = j + 0.5$, where j is an integer. Due to this symmetry, there are only two possible values for the translational offset x_0,

$$x_0 \in \left\{ -\frac{b}{2}, K(k) - \frac{b}{2} \right\}, \tag{19}$$

where $K(k)$ is the half period of the density. The offset forces the density in the center of each site to be either a minimum or a maximum of the site, depending on the sign of the interaction.

Since it is computationally intensive to include the integral in the wave number equation (16) with a root-finding algorithm, one of the parameters b, k, or B is varied while the other two are determined from the number equation (9) and boundary condition, Eq. (10). The offset is then choosen depending on which energy band is being examined. The wave number and energy are evaluated from these parameters and can then be plotted parametrically. In the following section, we discuss the energy bands for repulsive and attractive interatomic interactions.

III. NONLINEAR BAND STRUCTURE

The structure of the energy bands is strongly dependent on the strength and sign of the atom-atom interactions, g. In this section, the band structure is examined in all four parameter regimes: weakly repulsive, strongly repulsive, weakly attractive, and strongly attractive. Note that in this paper, a weakly interacting system is defined by $gn/V_0 \leqslant 1$ and a strongly interacting system is defined by $gn/V_0 \gg 1$

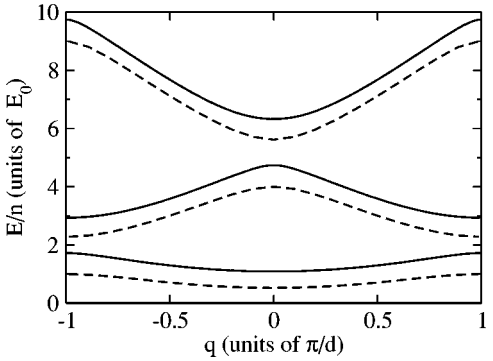

FIG. 1. Energy per particle as a function of the quasimomentum for the first three bands of a weakly repulsive condensate ($gn = E_0$) in a repulsive lattice ($V_0 = E_0$). The noninteracting, linear band structure is given by the dashed curves.

In Figs. 1 and 2, the energy bands for specific cases of weak and strong repulsive interactions are presented, $gn = E_0$ and $gn = 10E_0$, respectively. The condensates are assumed to be in a repulsive lattice, $V_0 = E_0$. In Fig. 1, the interaction strength is small and deviations from the linear band structure are small as well. The bands are vertically shifted higher as compared to a linear system due to the repulsive interactions, which increase the energy of the system. When the interaction strength is further increased the band structure becomes quite different. *Swallowtails* [30], or loops structures, appear in the bands, as in Fig. 2. The swallowtails appear at the edge of the Brillouin zones in the odd bands and at the center in the even bands. The width of these swallowtails grows as the interaction strength is increased. Swallowtails are a general feature of a nonlinear system in a periodic potential [29] and appear for both repulsive and attractive interactions.

The presence of swallowtails is due to the hysteric behavior of the superfluid condensate. A thorough discussion of

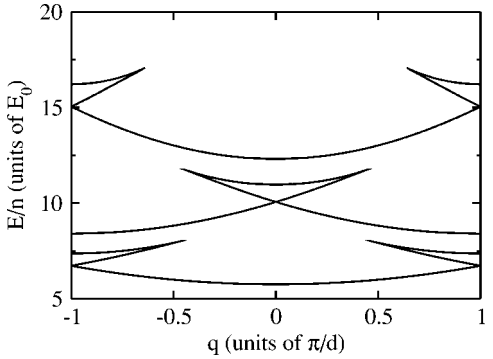

FIG. 2. Energy per particle as a function of the quasimomentum for the first three bands of a strongly repulsive condensate ($gn = 10E_0$) in a repulsive lattice ($V_0 = E_0$). Note the appearance of swallowtails at the edge of the Brillouin zone in the odd bands and at the center of the even bands.

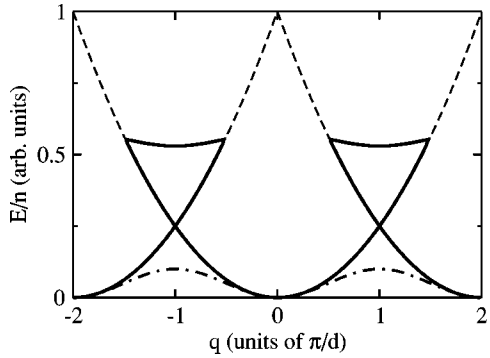

FIG. 3. Energy per particle as a function of the quasimomentum wave number for a noninteracting system with no potential (dashed curve), a periodic potential and small or no interaction (dot-dashed curve), and a periodic potential with a large interaction (solid curve).

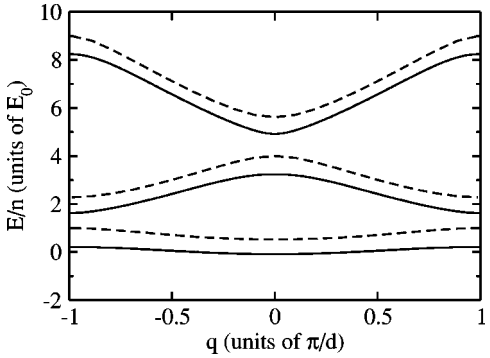

FIG. 4. Energy per particle as a function of the quasimomentum wave number for the first three bands of a weakly attractive condensate ($gn=-E_0$) in a repulsive lattice ($V_0=E_0$). The noninteracting linear band structure is given by the dashed curves.

this topic is given by Mueller [24] (see also references therein). For a completely free, noninteracting system, the energy has a quadratic dependence on the momentum, shown as the dashed parabolic curves in Fig. 3. Since a wave number of 2π leaves the system unchanged, the quadratic dependence is repeated centered around integer multiples of 2π. When a periodic potential is added to the system, bands in the energy are formed, shown as the dot-dashed sinusoidal curve in Fig. 3. These bands may be found by solving the linear Schrödinger equation. An interacting condensate, however, is a superfluid and can therefore screen out the periodic potential [39]. The energy band will then appear similar to that of a free particle, shown as a solid swallowtail curve in Fig. 3, until a critical point. At the critical momentum, determined by the average condensate sound speed, the energy band terminates. If this velocity allows the wave number to pass the edge of the Brillouin zone, there are then two separate energy minima. This demands that there be a saddle point separating them and hence the three stationary states.

For interacting systems in periodic potentials, there is a minimum interaction strength for which the swallowtails in the energy bands can exist [24]. This can, in general, be dependent on both the strength of the potential as well as the band that is being discussed. For a sinusoidal lattice it was shown that the onset of the swallowtail for the lowest band of a repulsive condensate occurs when the interaction strength and the potential are equal. For higher bands the relationship no longer becomes analytic [23]. For the Kronig-Penney lattice potential, the critical value for the onset of the swallowtails is not dependent on the band under consideration or the sign of the interaction. Numerically, we are able to determine that the onset occurs when $gn=2V_0$. This holds true in all cases except for the lowest band of an attractive condensate, as will be explained later in this section.

The energy bands are slightly different when the condensate is in an attractive potential, i.e., $V_0<0$. At the Brillouin zone boundary, the energy gap between bands is proportional to V_0 for a weakly interacting system. The second band then can cross the first band. In contrast, the bands are separated by an energy $\rho(0)V_0$ for a repulsive potential. As the interaction strength increases, the effects of the potential become less noticeable and the bands are no longer degenerate. Note that repulsive and attractive sinusoidal potentials create the same band structure. The difference in the current system arises since there are two length scales associated with a Kronig-Penney potential: the lattice spacing and δ function "width."

The energy bands for an attractive condensate in a repulsive potential, $V_0=E_0$, with a small interaction strength, $gn=-E_0$, have a qualitatively similar form as for a weakly repulsive condensate; see Fig. 4. Note that the attractive bands are, however, lower in energy than the repulsive bands due to the attractive interaction strength. A strongly attractive condensate, however, has several qualitative differences compared to a strongly repulsive condensate.

In Fig. 5, the band structure for a large attractive interaction, $gn=-10E_0$, in a repulsive potential, $V_0=E_0$, is illustrated. The swallowtails in the bands are now on the upper band at the band gaps as opposed to the lower bands at the band gaps as they were for the repulsive case in Fig. 2. The first energy band never has a swallowtail because the swal-

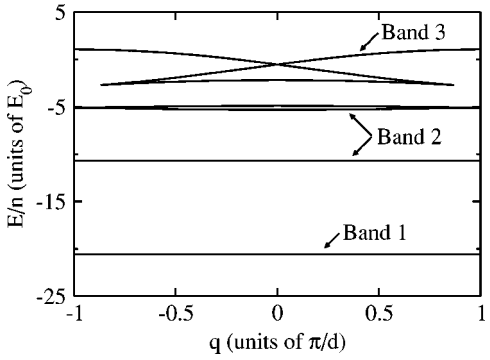

FIG. 5. Energy per particle as a function of the quasimomentum wave number for the first three bands of a strongly attractive condensate ($gn=-10E_0$) in a repulsive lattice ($V_0=E_0$). The first band does not have a swallowtail. However, the second and third bands do have swallowtails. The swallowtail in the second band appears as a loop with an unattached curve since an attractive condensate has a maximum width for the swallowtails, which in the case of the second band is a width of π.

lowtail must be on the lower portion of the band and below the center of the band there is no quadratic energy dependence for the swallowtail to follow; see Fig. 3.

The higher bands of a strongly interacting attractive condensate can look quite different than those of a strongly interacting repulsive condensate. For an attractive condensate, after the initial critical value of the interaction strength is reached, a swallowtail in the band starts to form, as in the third band of Fig. 5. As the interaction strength increases, another critical value is reached where the width of the swallowtail in q reaches π and runs into the band edge. Eventually, the wave number that should be less than zero becomes imaginary due to the form of α. This represents a nonphysical solution and is contrary to the assumption that the phase is real in Eq. (8). Therefore, the band appears as two separate curves: a loop and a separate line. These are both marked as band 2 in Fig. 5. It takes on this appearance since the swallowtail cannot extend lower than the minimum in the adjacent quadratic energy dependence. In general, the nth band will develop this two-part structure when the swallowtail reaches a width of $(n-1)\pi$ since the swallowtail will then have reached the minimum of the corresponding free particle energy. Note that this phenomenon does not occur for a repulsive interaction since there is no extremum to limit the growth of the swallowtail.

IV. DENSITY PROFILES

As density is the primary experimental observable for BEC's, the change in the density profile as the wave number is varied is important. The case of weak interactions creates similar changes in the density profile and energy band structure independent of the sign of the interaction. This is because the interaction energies are less than or of the same magnitude as the potential. For strong interactions, the density is in general more sharply peaked for an attractive condensate and flatter for a repulsive condensate. However, the general way in which the density changes is qualitatively similar.

The density changes in the first band of the weakly attractive condensate are shown for three different quasimomenta in Fig. 6. The solid curve, dashed curve, and dotted curve represent the density profile for $q=0$, $q=\pi/2$, and $q=\pi$, respectively. To understand the energy bands in terms of the density profile, the three terms of the energy in Eq. (17) should be discussed. The kinetic, interaction, and potential energies per particle are given by the first, second, and third terms of Eq. (17). Notice that the density at the origin monotonically decreases as the wave number is increased. Therefore the potential energy will also monotonically decrease due to the δ function at $x=j$, where j is an integer. Because the condensate is attractive, the interaction energy decreases monotonically as the wave number is increased since the density becomes more peaked. The kinetic energy monotonically increases as the wave number increases since the variations in the density become larger.

The case of the density variations associated with the first band of a strongly interacting repulsive condensate is shown in Fig. 7 and is qualitatively similar to that of the weakly attractive case. The solid curve represents the density profile for $q=0$. The dot-dashed curve represents the density when

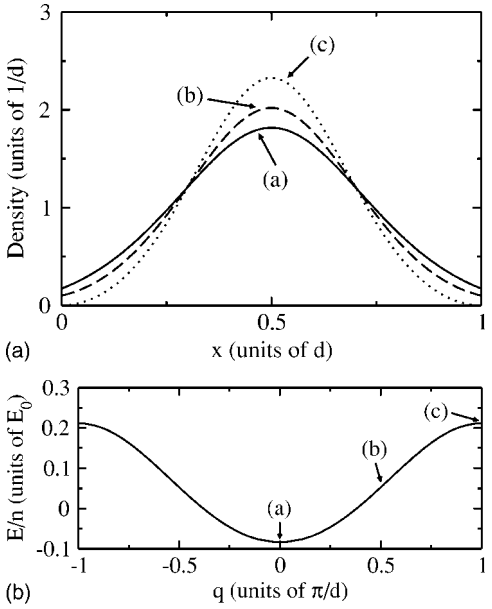

FIG. 6. Changes in the density of a weakly attractive, $gn=-E_0$, condensate associated with different positions on the first band. The solid curve represents the density when $q=0$. The dashed curve represents the density when $q=\pi/2$. The dotted curve represents the density when $q=\pi$. The lower plot shows the corresponding positions on the first energy band.

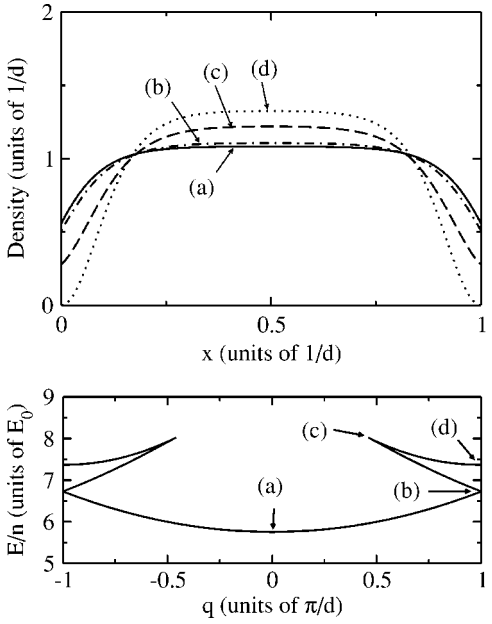

FIG. 7. Changes in the density of a strongly repulsive condensate, $gn=10E_0$, associated with different positions on the first band. The solid curve represents the density when $q=0$. The dot-dashed curve represents the density when $q=\pi$ at the bottom of the swallowtail. The dashed curve represents the density when $q=0.46\pi$ at the end of the swallowtail. The dotted curve represents the density when $q=\pi$ at the top of the swallowtail. The lower plot shows the corresponding positions on the first energy band.

$q=\pi$ at the bottom of the swallowtail. The dashed curve represents the density when $q=0.46\pi$ at the end of the swallowtail. The dotted curve represents the density when $q=\pi$ at the top of the swallowtail. The density at the origin again monotonically decreases as the wave number increases and therefore the potential energy also increases monotonically. The interaction energy increases monotonically as the band is traversed since the density becomes more peaked. The kinetic energy follows the same qualitative path as the total energy. Of the three, it is therefore the kinetic energy that has the greatest influence on the energy bands.

V. STABILITY

We proceed to study the stability of the Bloch states and to determine the stable regions of the bands. In addition to stable solutions, solutions that have instability times much longer than experimental time scales can be observed in experiments. Recent studies of the stability of condensates in a periodic potential have focused on linear energetic and dynamic stability, also called Landau stability [10,23,31,47,55]. In contrast, we consider the full response of the condensate to stochastic perturbations. In order to numerically simulate the NLS with a periodic potential, a ring geometry was used with a quantized phase such that $Nq=2\pi j$, where q is the wave number, N is the number of sites, and j is an integer. To ensure that the phase quantization did not effect the stability properties, enough lattice sites were used to allow for many rotations of the phase. The outcome of the stability analysis was independent of the number of sites for sufficiently large number of sites. In most cases, $j=4$ was found to be adequate to extract the correct stability properties.

The δ functions were simulated by single-point distortions in the potential grid. They were also implemented by using boxes of different widths with their area normalized to create the appropriate potential strength. The size of the boxes did not influence the stability properties until the width became approximately 10% of the healing length

$$\xi \equiv 1/\sqrt{2gn}, \tag{20}$$

where the length is scaled by the lattice spacing d.

The NLS was evolved using a variable-step fourth-order Runge-Kutta algorithm in time and a filtered pseudospectral method in space. The noise introduced into the simulations comes from double precision round-off error. To ensure that the form of the noise from the round-off error did not affect the stability properties of the system, initial stochastic white noise of various levels was introduced into the Fourier spectrum. For levels significantly greater than the round-off noise, the stability times approached those from the round-off noise. The introduction of white noise at the level in the 8th significant digit produced the same instability times as the round-off noise, which effects the 16th significant digit. All simulations were performed over time scales longer than experimental lifetimes of the BEC, which are typically 1–100 seconds.

The time at which the onset of instability occurs is determined by the effective variance in the Fourier spectrum,

$$\sigma(t) \equiv \sqrt{\frac{\sum [f(p,t)-f(p,0)]^2}{2\sum [f(p,0)]^2}}, \tag{21}$$

where $f(p,t)$ is the Fourier component of the wave function at momentum p and time t and the sum is over the momentum grid. This quantity determines how different the Fourier spectrum is compared to the original stationary state. It vanishes when the two spectra are identical and approaches unity when there are no Fourier components in common. When $\sigma(t)$ reaches 0.5, i.e., when 50% of the Fourier spectrum is different than the original, we consider the system is have become unstable.

Unless otherwise noted, for the stability analysis the lattice spacing is given by $d=1$ μm, the approximate length scale with which current optical lattices are created. In addition, all instability time scales will be given for ^{87}Rb.

A. Attractive atomic interactions

With an attractive interaction of $gn=-E_0$ in a repulsive potential of $V_0=E_0$ (see Fig. 4), the lowest-energy solution, zero quasimomentum in the lowest band, has a lifetime greater than experimental time scales. However, when even a slight harmonic perturbation to the potential is added to the initial time step the condensate becomes rapidly unstable. For instance, with a harmonic frequency of 120 Hz, which is approximately the experimental trapping frequency [56], simulations show an instability at 1.5 ms. This is short compared to the lifetime of a BEC [56], but still observable.

When the quasimomentum of the first band is increased, the stability of the system becomes dependent on the effective mass. The effective mass m^* is defined as [57],

$$m^* \equiv \frac{1}{\partial^2 E/\partial q^2}. \tag{22}$$

The physical meaning of the effective mass is the mass that the particle would appear to have if the potential was not being considered [1]. The sign of the effective mass can be transferred to the interaction strength, changing an attractive interaction to an effective repulsive interaction. Therefore, when the quasimomentum increases and the energy band becomes concave down, $m^*<0$, the system enters a regime of stability. The system remains stable even in the presence of the harmonic perturbation.

For zero quasimomentum in the second band, the system immediately develops temporally periodic variations in the phase and density. There is an additional instability, occurring on the order of 5 ms, that destroys the periodicity of the system. One might expect that this part of the band be stable since there is a negative effective mass but the oscillations due to the two density peaks per lattice site cause the system to be unstable. The oscillations, although periodic in time, create a larger underlying instability.

The stability properties of a strongly attractive condensate are similar to those of a weakly attractive condensate. The stability of the first band is determined by the effective mass while higher bands always go unstable. Therefore, for an attractive condensate, the system of Bloch waves is stable

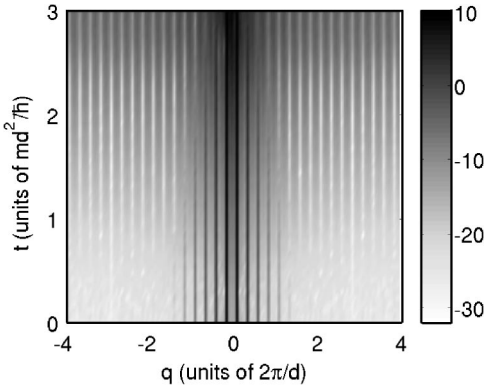

FIG. 8. Logarithm of the Fourier spectrum during the time evolution. Time is in units of $\hbar/E_0$ and distance in units of the lattice spacing.

only if there is one density peak per lattice site and the effective mass is negative.

B. Repulsive atomic interactions

Like an attractive condensate, a repulsive condensate only has stable regions on the first band. For a weakly interacting repulsive condensate, $gn=E_0$ and $V_0=E_0$, the effective mass in the first band is positive between $q=0$ and $q=\pi/2$. The effective mass becomes negative for larger quasimomentum, since the energy becomes concave down. Hence the system becomes unstable. For a wave number of $q=9\pi/16$ the instability time is 10 ms. This decreases to 2 ms for $q=\pi$. In this regime, with negative effective mass, the actual ground state is an envelope soliton that can spread over many lattice sites. These types of states are called gap solitons [9,28,37,58] and only occur in interacting systems. A gap soliton cannot be described by the Bloch ansatz. Figure 8 presents the unstable evolution of the weakly repulsive condensate in the first band with a wave number of $q=\pi$ in Fourier space. Notice that the instabilities arise from perturbations around the primary Fourier components of the wave function. In Fig. 9, the effective variance σ is plotted as a function of evolution time. The system becomes unstable

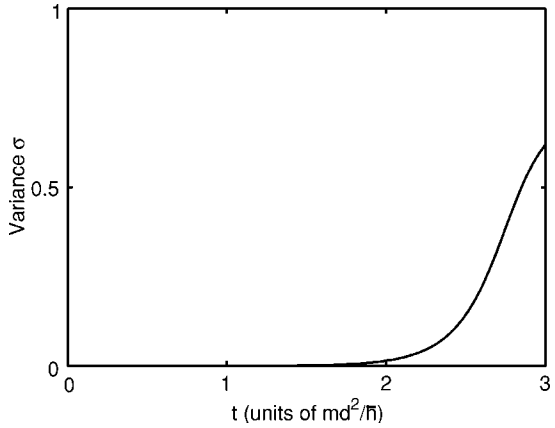

FIG. 9. The time evolution of the effective variance of the momentum density, σ. Time is in units of $\hbar/E_0$.

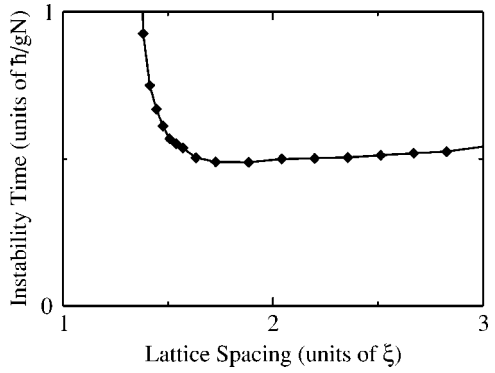

FIG. 10. The instability time as the lattice spacing is varied. Time is in units of $\hbar/gn$ and distance in units of the healing length, $\xi=d/\sqrt{2gn}$. Diamonds represent results of numerical simulations while the curve is a guide to the eye.

around 2 ms. The second band becomes unstable in 0.5 ms for $q=0$ and in 6 ms for $q=\pi$. Therefore, the system is stable in the first band with positive effective mass and unstable elsewhere. This is consistent with the effects that the effective mass has on stability in systems described by the lowest band DNLS. In a work by Fallani *et al.* [10], the instability time of a condensate in a lattice was measured by using an rf shield to remove the hottest atoms produced by the heating created in the sample by instability. The loss rate, equal to the inverse of the lifetime, should then be qualitatively similar to the instability time. Our calculations are consistent with these experimentally observed loss rates of a BEC in an optical lattice [10].

Due to the presence of the swallowtails, the strongly interacting system provides different stability regimes. For a repulsive condensate with $gn=10E_0$, in a repulsive lattice with $V_0=E_0$, the main section of the first band, as well as the lower portion of the swallowtail, has positive effective mass and remains stable. The upper portion of the swallowtail, as discussed in Sec. III, is an energy maximum and is not expected to remain stable. Our simulations find that the instability time of the upper portion of the swallowtail is approximately 0.2 ms, independent of the actual quasimomentum.

The size of the lattice spacing can influence the time scales for which the system becomes unstable. In Fig. 10, the instability time is presented as a function of the lattice spacing for a repulsive condensate, $gn=E_a$, in a repulsive lattice, $V_0=E_a$, with a wave number of $q=\pi$, where $E_a \equiv \hbar^2\pi^2/2m(1\ \mu\text{m})^2$.

There is a minimum instability time as the lattice spacing varies that occurs when the lattice spacing is approximately twice the healing length ξ. The instability time is given by half of the interaction strength time, $gn/\hbar$. When the lattice spacing is much larger than the healing length, the density becomes extremely flat except at the δ functions, where the density deformations take the form of pinned dark solitons. Since the lattice spacing is large, the dark solitons are far apart and are effectively noninteracting pinned solitons. Dark solitons are known to be robustly stable [32,59]. Therefore, for a lattice spacing much larger than the healing length the system becomes stable. For lattice spacing smaller than about twice the healing length, the condensate does not dis-

tinguish between the separate δ functions and sees closer to a constant potential. In this regime, the kinetic energy becomes much greater than the interaction energy and potential energy since variations in the density occur on the length scale of $d/2$, which is less than the healing length. The system becomes effectively free and noninteracting and, therefore, approaches stability.

VI. DISCUSSION AND CONCLUSIONS

The full set of Bloch wave stationary states of a Bose-Einstein condensate in a Kronig-Penney lattice potential, with period commensurate with the lattice, has been presented analytically for both repulsive and attractive interactions. The quasimomentum energy bands were found to exhibit a cusp at the critical interaction strength $gn=2V_0$, where g is the interatomic interaction strength, n is the number of atoms per well, and V_0 is the lattice potential strength. For larger interaction strengths, swallowtails form in the bands. These swallowtails have the same qualitative form as for a sinusoidal potental and exhibit the same stability properties.

Both attractive and repulsive condensates were found to be dynamically stable only in the first band and when the effective interaction, $\mathrm{sgn}(m^*)g$, was positive. Also, even in the first band, the upper edges of the swallowtails were always unstable. Therefore, for an attractive condensate, the only stable Bloch states exist in the first band between the quasimomentum where m^* becomes negative and $q=\pi$. A repulsive condensate is only stable in the first band from $q=0$ to the quasimomentum where m^* becomes negative. Higher bands are always unstable, for both attractive and repulsive condensates. When solutions became unstable, our numerical studies consistently observed that the instabilities originated around the primary Fourier components of the wave function. This is in agreement with the formal proof of the instability of constant-phase Bloch-wave solutions by Bronski *et al.* [32]. The instability time was found to be a function of the lattice constant. If the δ functions are spaced either much smaller than or much larger than the healing length of the condensate, the solutions had instability times longer than the lifetime of the BEC. Thus experiments could access formally unstable sections of the energy bands and, by controlling the ratio of the healing length to the lattice constant, directly observe the dynamics of instability. The results of our stability analysis are consistent with the experimental work performed by Fallani *et al.* [10], in which the loss rate, the inverse of the lifetime, was determined by removing the hottest atoms with an rf shield.

An interesting phenomenon to note is that for a repulsive condensate when a swallowtail is present, the entire energy band is concave up and, hence, the effective mass is always positive. This is in contrast to a weakly repulsive condensate, when the concavity of the energy band changes, creating a region of negative effective mass. Therefore, there is a maximum interaction strength for which gap solitons [3,9,28,37,58] can be formed since they require a negative effective mass. For the Kronig-Penney potential the maximum interaction energy is given by $gn=2V_0$, the strength at which swallowtails appear.

It should be noted that the solutions given in the paper map onto both the linear Schrödinger equation and discrete nonlinear Schrödinger (DNLS) equation limits if the proper procedure is followed. In the limit that

$$\lim_{g,k\to 0} k^2/g \to A/b^2, \tag{23}$$

the linear dispersion relation for the linear Schrödinger equation is recovered. In the limit that

$$\frac{V_0}{gn} \gg 1, \tag{24}$$

one obtains the DNLS equation

$$i\partial_t \psi_j = \epsilon_j \psi_j + J_j(\psi_{j+1} + \psi_{j-1}) + U_j|\psi_j|^2\psi_j, \tag{25}$$

where ϵ_j, J_j, and U_j are obtained via the Wannier formalism [41].

Stationary solutions to the NLS with a Kronig-Penney potential need not take the form of Bloch states. Solutions with a period which is an integer multiple of the lattice period have been shown to exist for the sinusoidal potential [55] and are expected also to be present for the Kronig-Penney potential. Envelope solutions, such as gap solitons, also play an important role in other systems modelled by the NLS and have been observed in BEC's [9]. The analytic methods which we have described here are equally applicable to these solution types and will form the subject of future study [60].

ACKNOWLEDGMENTS

We acknowledge helpful discussions with John Cooper, Chris Pethick, Ana Maria Rey, Augusto Smerzi, and Eugene Zaremba. Support is acknowledged for B.T.S. from the National Science Foundation and for L.D.C. and M.J.H. from the U.S. Department of Energy , Office of Basic Energy Sciences via the Chemical Sciences, Geosciences and Biosciences Division.

[1] S. L. Altmann, *Band Theory of Metals: The Elements* (Pergamon Press, Oxford, 1970).
[2] R. A. Usmanov and L. B. Ioffe, Phys. Rev. B **69**, 214513 (2004).
[3] D. N. Christodoulides, F. Lederer, and Y. Silberberg, Nature (London) **424**, 817 (2003).
[4] M. Greiner, I. Bloch, O. Mandel, T. W. Hansch, and T. Esslinger, Appl. Phys. B: Lasers Opt. **73**, 769 (2001).
[5] M. Greiner, O. Mandel, T. Esslinger, T. W. Hansch, and I. Bloch, Nature (London) **415**, 39 (2002).
[6] L. Fallani, F. S. Cataliotti, J. Catani, C. Fort, M. Modugno, M. Zawada, and M. Inguscio, Phys. Rev. Lett. **91**, 240405 (2003).

[7] B. Eiermann, P. Treutlein, T. Anker, M. Albiez, M. Taglieber, K.-P. Marzlin, and M. K. Oberthaler, Phys. Rev. Lett. **91**, 060402 (2003).
[8] T. Esslinger and K. Molmer, Phys. Rev. Lett. **90**, 160406 (2003).
[9] B. Eiermann, T. Anker, M. Albiez, M. Taglieber, P. Treutlein, K. P. Marzlin, and M. K. Oberthaler, Phys. Rev. Lett. **92**, 230401 (2004).
[10] L. Fallani, L. De Sarlo, J. E. Lye, M. Modugno, R. Saers, C. Fort, and M. Inguscio, Phys. Rev. Lett. **93**, 140406 (2004).
[11] B. P. Anderson and M. A. Kasevich, Science **282**, 1686 (1998).
[12] E. W. Hagley, L. Deng, M. Kozuma, J. Wen, K. Helmerson, S. L. Rolston, and W. D. Phillips, Science **283**, 1706 (1999).
[13] Y. B. Ovchinnikov, J. H. Müller, M. R. Doery, E. J. D. Vredenbregt, K. Helmerson, S. L. Rolston, and W. D. Phillips, Phys. Rev. Lett. **83**, 284 (1999).
[14] J. L. Roberts, N. R. Claussen, J. P. Burke, Jr., C. H. Greene, E. A. Cornell, and C. E. Wieman, Phys. Rev. Lett. **81**, 5109 (1998).
[15] A. Inouye, M. R. Andrews, J. Stenger, H.-J. Miesner, D. M. Stamper-Kurn, and W. Ketterle, Nature (London) **392**, 151 (1998).
[16] E. P. Gross, Nuovo Cimento **20**, 454 (1961).
[17] L. P. Pitaevskii, Zh. Eksp. Teor. Fiz. **40**, 646 (1961) [Sov. Phys. JETP **13**, 451 (1961).
[18] B. T. Seaman, L. D. Carr, and M. J. Holland, Phys. Rev. A **71**, 033609 (2005).
[19] M. M. Bogdan, A. S. Kovalev, and I. V. Gerasimchuk, Low Temp. Phys. **23**, 145 (1997).
[20] G. E. Astrakharchik and L. P. Pitaevskii, Phys. Rev. A **70**, 013608 (2004).
[21] A. Radouani, Phys. Rev. A **70**, 013602 (2004).
[22] B. Wu, R. B. Diener, and Q. Niu, Phys. Rev. A **65**, 025601 (2002).
[23] M. Machholm, C. J. Pethick, and H. Smith, Phys. Rev. A **67**, 053613 (2003).
[24] E. J. Mueller, Phys. Rev. A **66**, 063603 (2002).
[25] M. H. Anderson, J. R. Ensher, M. R. Matthews, C. E. Wieman, and E. A. Cornell, Science **269**, 198 (1995).
[26] K. B. Davis, M.-O. Mewes, M. R. Andrews, N. J. van Druten, D. S. Durfee, D. M. Kurn, and W. Ketterle, Phys. Rev. Lett. **75**, 3969 (1995).
[27] P. Meystre and M. Sargent III, *Elements of Quantum Optics*, 3rd ed. (Springer, Berlin, 1999).
[28] G. Lenz, P. Meystre, and E. M. Wright, Phys. Rev. A **50**, 1681 (1994).
[29] B. Wu and Q. Niu, Phys. Rev. A **61**, 023402 (2001).
[30] B. Wu and Q. Niu, Phys. Rev. A **64**, 061603(R) (2001).
[31] J. C. Bronski, L. D. Carr, B. Deconinck, and J. N. Kutz, Phys. Rev. Lett. **86**, 1402 (2001).
[32] J. C. Bronski, L. D. Carr, B. Deconinck, J. N. Kutz, and K. Promislow, Phys. Rev. E **63**, 036612 (2001).
[33] L. D. Carr, J. N. Kutz, and W. P. Reinhardt, Phys. Rev. E **63**, 066604 (2001).
[34] D. Diakonov, L. M. Jensen, C. J. Pethick, and H. Smith, Phys. Rev. A **66**, 013604 (2002).
[35] B. Deconinck, B. A. Frigyik, and J. N. Kutz, J. Nonlinear Sci. **12**, 169 (2002).
[36] P. Massignan and M. Modugno, Phys. Rev. A **67**, 023614 (2003).
[37] P. J. Y. Louis, E. A. Ostrovskaya, C. M. Savage, and Y. S. Kivshar, Phys. Rev. A **67**, 013602 (2003).
[38] A. M. Rey, K. Burnett, R. Roth, M. Edwards, C. J. Williams, and C. W. Clark, J. Phys. B **36**, 825 (2003).
[39] E. Taylor and E. Zaremba, Phys. Rev. A **68**, 053611 (2003).
[40] E. A. Ostrovskaya and Y. S. Kivshar, Phys. Rev. Lett. **92**, 180405 (2004).
[41] A. M. Rey, Ph.D. thesis, University of Maryland at College Park, 2004.
[42] M. A. Porter, P. G. Kevrekidis, and B. A. Malomed, Physica D **196**, 106 (2004).
[43] A. A. Sukhorukov and Y. S. Kivshar, Phys. Rev. Lett. **87**, 083901 (2001).
[44] A. A. Sukhorukov and Y. S. Kivshar, Phys. Rev. E **65**, 036609 (2001).
[45] S. Theodorakis and E. Leontidis, J. Phys. A **30**, 4835 (1997).
[46] Y. B. Gaididei, P. L. Christiansen, K. O. Rasmussen, and M. Johansson, Phys. Rev. B **55**, R13365 (1997).
[47] D. Taras-Semchuk and J. M. F. Gunn, Phys. Rev. B **60**, 13139 (1999).
[48] S. A. Alexander and R. L. Coldwell, Int. J. Quantum Chem. **86**, 325 (2002).
[49] W.-D. Li and A. Smerzi, Phys. Rev. E **70**, 016605 (2004).
[50] L. Salasnich, A. Parola, and L. Reatto, Phys. Rev. A **65**, 043614 (2002).
[51] L. D. Carr, M. A. Leung, and W. P. Reinhardt, J. Phys. B **33**, 3983 (2000).
[52] M. Olshanii, Phys. Rev. Lett. **81**, 938 (1998).
[53] *Handbook of Mathematical Functions*, edited by M. Abramowitz and I. A. Stegun, National Bureau of Standards (U.S. & GPO, Washington, D.C., 1964).
[54] L. M. Milne-Thomson, *Jacobian Elliptic Function Tables* (Dover, New York, 1950).
[55] M. Machholm, A. Nicolin, C. J. Pethick, and H. Smith, Phys. Rev. A **69**, 043604 (2004).
[56] H. Moritz, T. Stöferle, M. Köhl, and T. Esslinger, Phys. Rev. Lett. **91**, 250402 (2003).
[57] Note one can also define an effective mass associated with the chemical potential bands as in Li and Smerzi [49].
[58] K. M. Hilligsoe, M. K. Oberthaler, and K.-P. Marzlin, Phys. Rev. A **66**, 063605 (2002).
[59] Y. S. Kivshar and B. Luther-Davies, Phys. Rep. **298**, 81 (1998).
[60] B. T. Seaman, L. D. Carr, and M. J. Holland (unpublished).